Journal of the Korean Physical Society, Vol. 57, No. 2, August 2010, pp. 305∼310

Proton Radiography and Fast Electron Propogation Through Cylidericall Compressed Targets

R. Jafer, L. Volpe and D. Batani*
dipartimento di fisica "G.Occhialini, Università di Milano-Bicocca, Italy

M. Koenig, S. Baton, E. Brambrink and F. Perez
Laboratoire pour l'Utilisation des Lasers Intenses, Ecole Polytechnique France

F. Dorchies, J. J. Santos, C. Fourment, S. Hulin, P. Nicolai and B. Vauzour
Université de Bordeaux - CNRS - CEA, France

K. Lancaster, M. Galimberti, R. Heathcote, M. Tolley and Ch. Spindloe
RAL, STFC, UK

P. Koester, L. Labate and L. Gizzi
CNR, Pisa, Italy

C. Benedetti and A. Sgattoni
Dipartimento di fisica, University of Bologna, Italy

M. Richetta
University of Rome "Tor Vergata" Italy

J. Pasley
University of York UK

F. Beg, S. Chawla and D. Higginson
University of California San Diego, California, USA

A. MacKinnon and A. McPhee
Lawrence Livermore National Laboratory, California, USA

Duck-Hee Kwon and Yongjoo Rhee
Korea Atomic Energy Research Institute

(Received 2 February 2010, in final form 26 June 2010)

The paper describes the key points contained in the short term HiPER (High Power laser Energy Research) experimental road map, as well as the results of two phases of the experiment performed in "HiPER dedicated time slots. Experimental and theoretical results of relativistic electron transport in cylindrically compressed matter are presented. This experiment was achieved at the VULCAN laser facility (UK) by using four long pulse beams ($\sim 4 \times 50$ J, 1 ns, at 0.53 μm) to compress a hollow plastic cylinder filled with plastic foam of three different densities (0.1, 0.3, and 1 g cm^{-3}). In the first phase of the experiment, protons accelerated by a picosecond laser pulse were used to radiograph a cylinder filled with 0.1 g/cc foam. Point projection proton backlighting was used to measure the degree of compression as well as the stagnation time. Results were compared to those from hard X-ray radiography. Finally, Monte Carlo simulations of proton propagation in cold and compressed targets allowed a detailed comparison with 2D numerical hydro simulations. 2D simulations predict a density of 2-5 g cm^{-3} and a plasma temperature up to 100 eV at maximum compression. In the second phase of the experiment, a short pulse (10 ps, 160 J) beam generated fast

electrons that propagated through the compressed matter by irradiating a nickel foil at an intensity of 5×10^{18} Wcm^{-2}. X-ray spectrometer and imagers were implemented in order to estimate the compressed plasma conditions and to infer the hot electron characteristics. Results are discussed and compared with simulations.

PACS numbers: 52.38.Kd, 52.38.-r, 52.57.Kk, 52.57.-z
Keywords: Electron transport, Proton radiography, X-ray radiography, ICF.
DOI: 10.3938/jkps.57.305

I. INTRODUCTION

Many experiments have been done on inertial confinement fusion (ICF), and different diagnostics have been used [1] to follow the implosion of the target and to study the fast-electron transport inside warm and dense matter [2,3]. Until now, most of the experiments carried out on this subject were designed to study cold planar targets at solid density. Such low-density and/or cold targets may exhibit a different behaviour of the hot electrons passing through it, compared with the final design. In particular, the stopping power of fast electrons should be affected by the return current, linked to the collective effects. In order to get closer to this goal, we have performed an experiment to study the electron transport in cylindrically compressed matter, which is a useful geometry to infer different measurements [4]. This experiment was split into two parts: the first one to achieve and study the cylindrical compression. Proton radiography [5–8] was used in the first phase to record the implosion history of the cylindrical target. In parallel, we used X-ray Radiography to have a comparison. Simulations were made with the Monte Carlo (MC) MCNPX Code [9] using the density profiles of the imploded cylinder obtained with the 2D-hydro CHIC code [10,11]. Laser based protons are characterised by small source, high degree of collimation, short duration and a continuous spectrum upto a high-energy cut-off. Taking radiograph with multi-energetic protons allows the implosion history to be recorded in a single shot. This study is one of the key objectives within the HiPER roadmap.

Detailed hydrodynamics design was performed in preparation of the experiment. Figure 1 shows an example of a target used in the experiment (produced by the RAL target prep group). Four ns laser beams were perpendicularly focused on the plastic cylinder to drive its implosion.

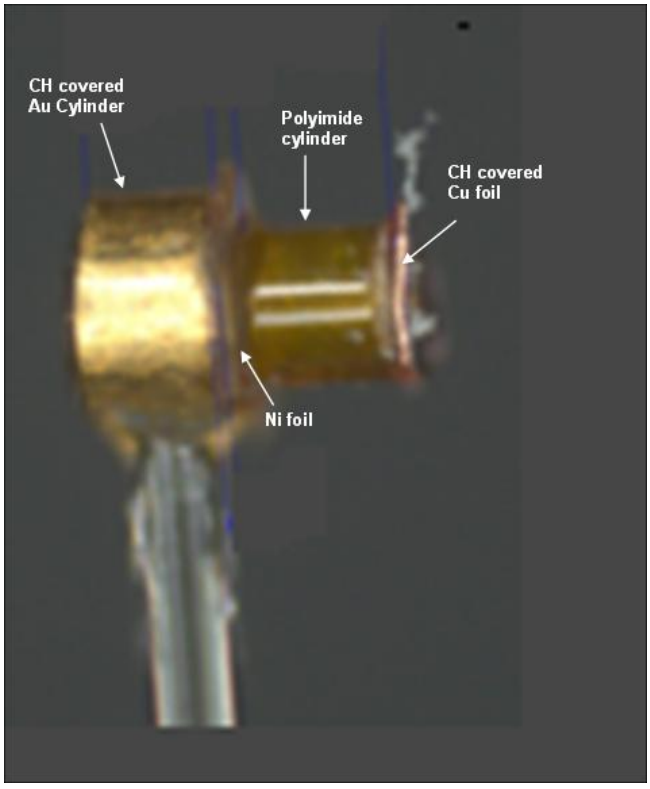

Fig. 1. Example of a target used in the experiment (thanks to Ch. Spindloe, M. Tolley and all the RAL target prep group).

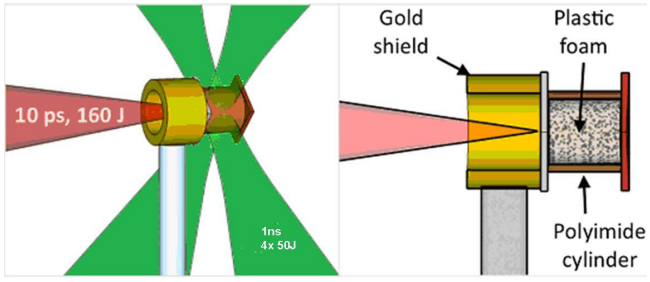

Fig. 2. Schematics of the target and the laser design.

II. EXPERIMENTAL SETUP

The experiment was performed at the VULCAN laser facility (UK). Four long-pulse laser beams (about 4×50 to 4×70 J in 1 ns) at 0.53 μm, focused to 150 μm FWHM spots through *hybrid* phase plates, were used to cylindrically compress a 200 μm long polyimide tube. This tube had a 220 μm outer diameter and a 20 μm wall thickness, as shown in Fig. 2.

The target was filled with plastic polymer (TMPTA) at different densities: 0.1 or 0.3 g cm^{-3} foam or 1 g cm^{-3} solid plastic. Both sides were closed with 20μm thick foils

*E-mail:

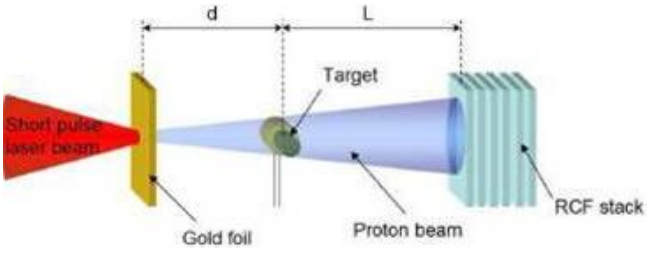

Fig. 3. Schematic of the proton radiography Setup.

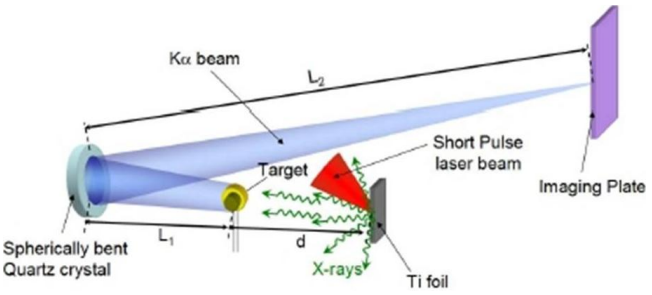

Fig. 4. Schematic of the x-ray radiography setup.

of Ni and Cu, respectively. To produce the hot electrons, an additional laser (160 J in 10 ps) was focused on the Ni layer at an intensity of $\sim 5 \times 10^{18}$ Wcm^{-2}, by using an $f/3$ off-axis parabola. In order to limit the alteration of the picosecond beam caused by the low-density plasma generated by the nanosecond pulses, a tube-shaped gold shield was stuck on the Ni foil. The four nanosecond beams were individually timed to hit the target with a precision better than 100 ps. The delay τ between the long pulses and the short pulse was adjustable from 0 to more than 3 ns with a jitter of $\pm$100 ps. At $\tau = 0$, the short pulse hit the target as the long pulses arrived. The experiment was split into two phases. The objective of the first phase was to determine the hydrodynamic characteristics of the compressed matter, i.e; its temperature and density at optimal compression. In order to determine some of the parameters of the compressed cylinder, an additional laser (100 J in 1ps, 20 μm FWHM) was focused on a 10 mm distant foil to make an x-ray or proton backlighter for the diagnostics. Transverse point-projection proton radiography [12] can be employed to infer the target density in shock-compressed targets. A proton source was produced by using the short pulse laser beam focused on 20 μm gold foil, placed 10mm away from the target. The detector was a radiochromic film (RCF) stack protected by a 12 μm thick Al foil, placed $\sim$50 mm away from the target. The stacks were composed of 5 HD and 10 MD RCFs as shown in Fig. 3.

Density measurements were also planned with an x-ray radiography diagnostic [13]. Using Ti foils 10mm away from the target as backlighters and a quartz crystal to reflect the Ti-Kα radiation (at 4.5 keV) that passed through the compressed target, we obtained a magnification of $\sim$10. In order to get sufficient absorption, the plastic foam was doped with 30% Cl in mass. The quartz crystal (interatomic distance of 1.374 Å) was spherically bent with a radius of curvature 380 mm. Imaging plates positioned $\sim$2 m away from this crystal detected the Ti-Kα radiation, as shown in Fig. 4.

The second phase of the experiment was designed to measure the hot electron propagation through the compressed matter. The plastic foam inside the cylinder was doped with 10 - 20% Cu in mass so as to get x-ray emission from this region. Two spherically bent quartz crystals with a 1.541Å interatomic distances and a radius of curvature of 380 mm provided 2D monochromatic images, using imaging plates as detector, around the Cu-Kα1 line, *i.e,* at 8050 $\pm$ 5 eV. These crystals were placed to have both side- and rear-view images of the cylinder with a magnification of $\sim$10 and a spatial resolution between 10 and 20 μm. Cylindrically bent quartz with a 1.012 Å interatomic distances and a radius of curvature of 100 mm, produced time- and space-integrated spectra for x-ray energies from 7.3 to 9.3 keV in a Von Hamos configuration. Both the Cu-Kα and Ni-Kα lines could be detected with a spectral resolution of 3 $\pm$ 2eV. A second spectrometer consisting of planar highly oriented pyrolitic graphite (HOPG) monitored the same emission lines with a much higher sensitivity [14], but a lower spectral resolution ($\sim$50 eV).

III. EXPERIMENTAL RESULTS

1. Radiography

The experimental proton radiographs of the reference cylinder and of the imploding cylinder at different stages of compressions are shown in Fig 5. The minimum observed diameter is $\sim$140 μm at 2.3 ns.

From the experimental analysis it seems that low energy protons are not able to probe the dense core as deeply as X-rays do as shown in Figs. 6(a) and (b). Protons seem to penetrate less than x-rays, that's why we needed to run MC simulations to recover the original size of the cylinder in proton radiography, which is shown in the Fig. 7. This can depend on many physical effects, among which the most important are the multiple scattering (MS) of protons with the atoms of the target and different behaviours of the proton stopping power (SP) while passing through a gradient of density (*e.g,* plasma temperature effects). In order to investigate all these physical effects we have run a "start to end" simulation of the process using Monte Carlo code prepared by LANL. In this code the SP and MS effects are taken into account respectively with Bethe [15] and Rossi [16] theories. Following the experimental analysis we have extracted FWHM by using Gaussian fits and in simulations we got the similar results as shown in Fig. 7, by taking into account the above mentioned physical effects.

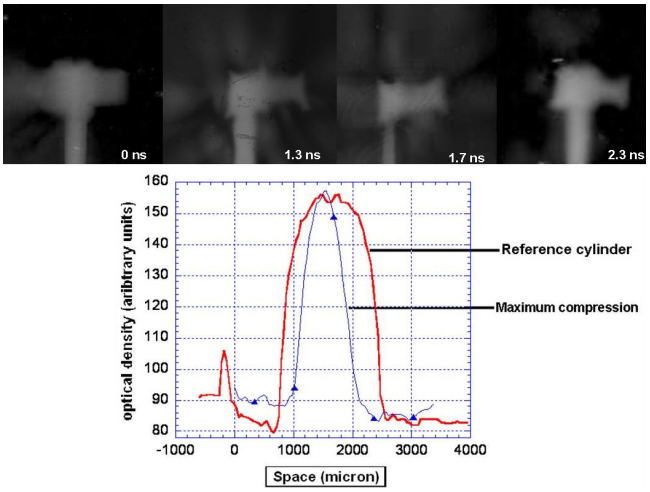

Fig. 5. (Color online) The top images are showing the compression history obtained by experimental proton radiographs at $t_1 = 0$ ns, $t_2 = 1.3$ ns, $t_3 = 1.7$ ns, and $t_4 = 2.3$ ns.The figure below shows the densitometries along the minimum diameters. The uncompressed plastic cylinder could be fitted with a supergaussian profile (red) while the compressed cylinder (blue) fitted with a gaussian shape.

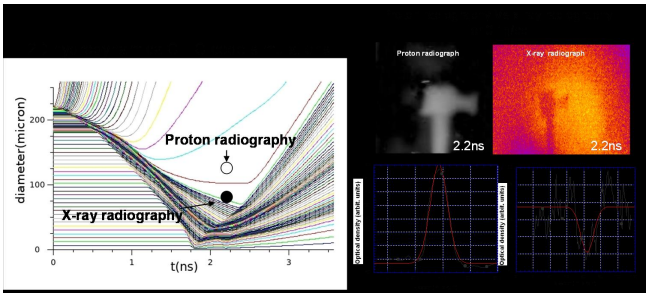

Fig. 6. (Color online) (a) the comparison of the compressions obtained with Proton and X-ray radiography with 2D hydrodynamic CHIC code simulations. (b) proton (left) and x-ray (right) radiographies of cylinder at maximum compression and corresponding optical densities profiles

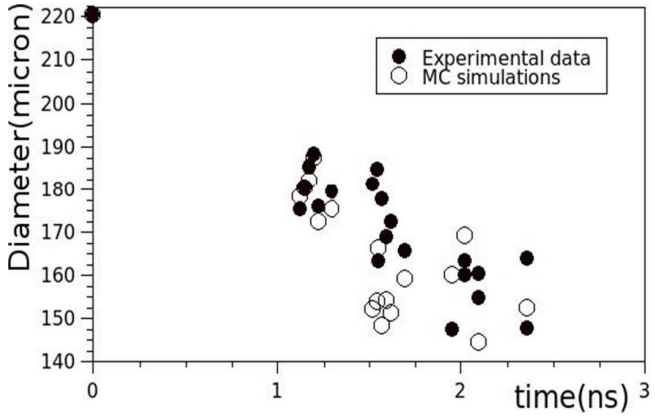

Fig. 7. Experimental and numerical points, the sets of data are in good agreement with each other

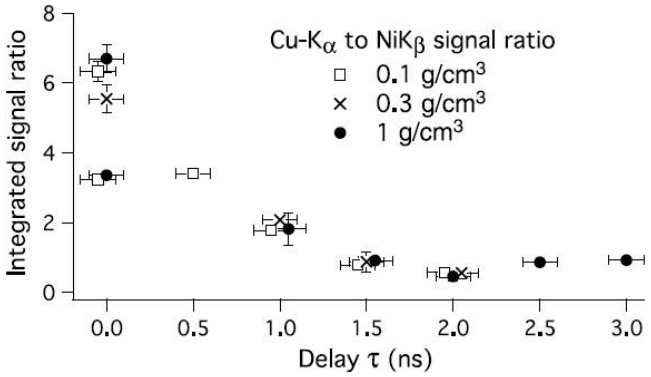

Fig. 8. Ratio between Cu and Ni x-ray emissions as measured with the HOPG spectrometer versus the delay , for different initial core densities.

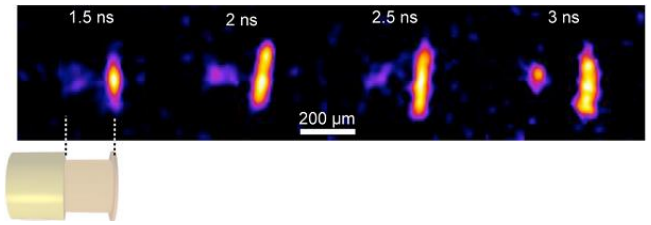

Fig. 9. (Color online) Side-view x-ray images of the Cu-Kα emission from the compressed cylinder at different delays (1 g cm^{-3} initial density in all cases).

2. Electron Propagation in cylindrically compressed targets

In the second phase of the experiment, the two x-ray spectrometers detected the K_α and the K_β emission from both Cu and Ni foils. The Ni emission is a good indicator of the electron source. The Cu signal indicates an electron population propagating through the target. The first interesting data are then the ratio between the Cu and the Ni signal as it indicates the fraction of the hot (>8 keV) electrons that reached the rear surface of the target. These data are presented in Fig. 8 for different delays, given by the HOPG spectrometer. There is a clear decrease up to $\tau = 2$ ns, after which the ratio is constant. Furthermore, this effect is identical for the three different initial core densities used. These results, discussed below, were validated for the other spectrometer and the two x-ray imagers.

The side-view x-ray imager produced images of the Cu-K_α emission from the rear Cu foil, and from the Cu doping inside the plastic core. In the four images of Fig. 9, the emission from the core is clearly differentiated that from the Cu foil. The vertical size of this core is about 50 μm at maximum compression, which is in agreement with the presented simulations. One can also easily see that the horizontal length of the emitting region inside the cylinder decreases with the delay: the penetration depth of the electrons is reduced for a high compression.

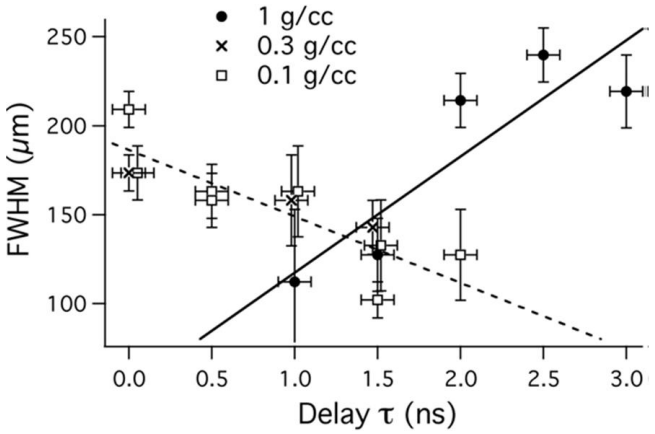

Fig. 10. Side-view imager results for fast-electron beam divergence measurements: rear surface foil width for different target densities. Linear fits are plotted for low- or high-density targets.

For low-density targets, the number of Cu atoms in the foam turned out to be too low to have a significant number of photons coming out of the target.

Now, taking into account the rear Cu foil instead of the core, the measurement of the width of this rear surface Cu-K_α emission is closely linked to the divergence of the electrons reaching the rear surface. The side-view x-ray imager corresponding results are plotted in Fig. 10. It shows two different behaviours of the hot electron divergence. With low-density targets, the width decreases with the delay. The opposite trend is observed for high-density targets.

IV. DISCUSSIONS AND CONCLUSIONS

Protons and x-rays have been used to diagnose the implosion of cylindrical targets. X-rays seem more penetrating in compressed targets than low energy protons. Simulations are, therefore needed to analyze the RCF images. Simulated data are able to approximately reproduce the observed size of the images on RCF experimental data. Taking radiographs with multi-energetic protons allows the implosion history to be recorded in a single shot. The protons do not seem to probe the dense core, but the implosion history and the stagnation time is revealed correctly. The higher proton energies are needed to probe the dense core.

The second phase results indicate a decreasing fraction of electrons reach the rear surface when the compression occurs. It shows that the electrons are slowed down more efficiently with a high compression. For delays above 2 ns, the signal shows a plateau, which hints at the presence of a hot electron component reaching the rear surface through the high-density core. This is supported by the side-view images of Fig. 9 as the same integrated signal is always visible on this rear surface. These images also confirm the presence of hot electrons inside the dense target.

To explain the electron divergence behaviour of Fig. 10, a few leads have to be investigated. We observe two different trends: the spot size either decreases or increases with the compression evolution. For the former case, we can formulate the following explanations. Firstly, the increasing density prevents the coldest electrons from reaching the rear surface. The remaining electrons, being more energetic, are less deviated through the plasma, resulting in a lower detected divergence. Secondly, the low-density targets are composed of a shell that is much denser than the core. The corresponding density ratio is about 5:1 at maximum compression, with a 50 μm diameter core. A resistivity model from [17] and the results from [18] applied to the present case could indicate a resistive confinement of the electrons inside the cylinder core, thus reducing the electron beam size while the cylinder is being compressed. Similarly, collision processes might be able to prevent the electrons from diverging through the dense shell. Lastly, the electron beam can be truncated by this shell (because of an increased stopping power) thus giving a smaller spot on the rear surface. All these guiding effects may not apply in the case of high-density (solid) targets. However, it is difficult to say whether they are able to reverse the trend, *i.e.*, divergence increasing with the delay. Indeed, measurements on such a small scale target make their interpretation difficult. To answer this question, electron transport simulations are under consideration.

In conclusion, cylindrical compression has been achieved and measured to be in good agreement with the hydrodynamic simulations, and the electron transport features have been measured. Within the fast-ignition framework, the presented results indicate that the same numbers of fast electrons able to reach the high-density region are observed for different initial target densities. More surprisingly, the electron divergence appears to depend strongly on the plasma geometries achieved for those different initial densities. In order to understand the above results, electron propagation simulations using electron transport codes still need to be performed. As one of the few experiments on electron transport in compressed matter [19], further studies need to be achieved to complete the HiPER roadmap. Overall, this experiment was an important test bed for the lasers and the diagnostics in such a new configuration, several challenging experimental points have been clarified, and fast-electron behaviours in compressed matter have been underlined.

REFERENCES

[1] P. E. Stott, A. Wootton, G. Gorini and D. Batani, *Advanced Diagnostics for Magnetic and inertial fusion* (Kluwer, Academic/Plenum Publishers, New York, 2002).

[2] T. A. Hall *et al.*, Phys. Plasmas **1**, 1626-34
[3] F. Perez M Koenig *et al.*, Plasma Phys. Controlled Fusion **51**, 124035 (2009).
[4] H. Nakamura *et al.*, Phys. Rev. Lett. **100**, 165001 (2008)
[5] P.-H. Maire and J. Breil, Int. J. Numer. Methods Fluids **56**, 1417 (2008).
[6] A. J. Mackinnon *et al.*, Phy. Rev. Lett. **97**, 045001 (2006).
[7] M. Borghesi *et al.*, Plasma phys. Controlled Fusion **43**, A267 (2001).
[8] R. Jafer *et al.* "Proton Radiography of a cylindrical Laser-Driven Implosions" ULIS proceedings volume, (2009).
[9] Nucl. Instrum. Methods Phys. Res. A **580**, 110 (2007).
[10] C. K. Li *et al.*, Phy. Rev. Lett. **100**, 225001 (2008).
[11] P. H. Maire, J. Breil, R. Abgral and J. Ovadia, SIAM SISC, 1781 (2007).
[12] S. Pape *et al.*, High Energy Density Phys. **2**, 1 (2006).
[13] A. Benuzzi-Mounaix *et al.*, Phys. Rev. E **77**, 045402 (2008).
[14] H.-S. Park *et al.*, Rev. Sci. Instrum. **75**, 3747 (2004).
[15] G. Moliere, Z. Naturfosh, 2a, 133 (1947); 3a, 78 (1948) . H. A. Bethe, Phys. Rev. 89 1256 (1953); W. T. Scott, Rev. Mod.
[16] B. Rossi and K. Greisen, Rev. Mod. Phys. **13**, (1941).
[17] Y. T. Lee and R. M. More, Phys. Fluids **27**, 1273 (1984).
[18] S. Kar, A. P. L. Robinson, D. C Carroll, O Lundh, K. Markey, P. McKenna, P. Norreys and M. Zepf, Phys. Rev. Lett. **102**, 055001 (2009).
[19] T. A. Hall *et al.*, Phys. Rev. Lett. **81**, 1003 (1998).